

## Identification and Diagnosis of Asynchronous Motor Imbalance Faults Using Surrogate Models

Özgür AYDIN<sup>1\*</sup> , Erhan AKIN<sup>2</sup> 

<sup>1</sup> Bingöl University, Informatics Department, Bingöl, Türkiye

<sup>2</sup> Fırat University, Engineering Faculty, Elazığ, Türkiye

Özgür AYDIN ORCID No: 0000-0001-8130-277X

Erhan AKIN ORCID No: 0000-0001-6476-9255

\*Corresponding author: [iamozguraydin@gmail.com](mailto:iamozguraydin@gmail.com)

(Received: 15.01.2025, Accepted: 28.04.2025, Online Publication: 27.06.2025)

### Keywords

Asynchronous motor fault diagnosis, Surrogate model, Imbalance fault, Vibration analysis, Multi-Model classification

**Abstract:** Asynchronous motors have a wide range of industrial applications due to their robust structure, low maintenance costs, and high reliability. However, these motors can be exposed to electrical and mechanical faults caused by environmental and operational conditions. Among the types of faults are problems such as bearing failures, stator winding faults, and rotor bar breakages, with mechanical imbalance faults standing out as a critical issue that adversely affects motor performance. This study aims to compare the performance of surrogate models (RBF and KRG) and deep learning models (RNN, GRU, LSTM), which represent a novel approach for diagnosing imbalance faults in asynchronous motors. For this purpose, experimentally collected current ( $I_a$ ,  $I_b$ ,  $I_c$ ) and vibration ( $X$ ,  $Y$ ,  $Z$ ) signals were analyzed in the frequency domain, and the features obtained via FFT were used in classification processes for three classes (Healthy, DA\_1, DA\_2). According to the results, the RBF model exhibited the best performance with an accuracy of 97.78% and a precision of 97.64%, while the KRG model showed remarkable success with an accuracy of 93.89% and a precision of 93.71%. In contrast, the deep learning models with the highest accuracy, RNN and LSTM, demonstrated lower performance with an accuracy of 87.22% and a precision of 87.23%. Compared to the RNN model, which is the most accurate deep learning model, the RBF model achieved an improvement of 12.11% in accuracy and 11.93% in precision, proving to be a superior tool in diagnosing imbalance faults. Notably, it achieved 100% accuracy in the DA\_2 class and distinguished itself from other classes with its distinct features. These findings show that surrogate models offer an effective solution in asynchronous motor fault diagnosis by providing high accuracy and precision rates along with limited data requirements and low computational cost.

## Asenkron Motor Dengesizlik Arızalarının Vekil Modellerle Tanımlanması ve Teşhisi

### Anahtar Kelimeler

Asenkron motor arıza teşhisi, Vekil model, Dengesizlik arızası, Titreşim analizi, Çoklu model sınıflandırma

**Öz:** Asenkron motorlar, sağlam yapıları, düşük bakım maliyetleri ve yüksek güvenilirlikleri ile endüstride geniş bir kullanım alanına sahiptir. Ancak, bu motorlar çevresel ve operasyonel koşullardan kaynaklanan elektriksel ve mekanik arızalara maruz kalabilmektedir. Arıza türleri arasında rulman problemleri, stator sargı hataları ve rotor çubuğu kırılmaları gibi sorunlar yer almakta, özellikle mekanik dengesizlik arızaları motor performansını olumsuz etkileyen kritik bir sorun olarak öne çıkmaktadır. Bu çalışma, asenkron motorlarda dengesizlik arızalarının teşhisi edilmesine yönelik yeni bir yaklaşım olan vekil modeller (RBF ve KRG) ile derin öğrenme modellerinin (RNN, GRU, LSTM) performansını karşılaştırmayı amaçlamaktadır. Bu amaçla, deneysel olarak toplanan akım ( $I_a$ ,  $I_b$ ,  $I_c$ ) ve titreşim ( $X$ ,  $Y$ ,  $Z$ ) sinyalleri, frekans alanında analiz edilmiş ve FFT ile elde edilen özellikler, üç sınıf (Sağlıklı, DA\_1, DA\_2) için sınıflandırma süreçlerinde kullanılmıştır. Sonuçlara göre, RBF modeli, %97.78 doğruluk ve %97.64 keskinlik oranı ile en iyi performansı sergilemiş, KRG modeli ise %93.89 doğruluk ve %93.71 keskinlik oranı ile dikkate değer bir başarı göstermiştir. Buna karşılık, derin öğrenme modellerinden en yüksek doğruluk oranına sahip olan RNN ve LSTM

%87.22 doğruluk ve %87.23 keskinlik oranı ile daha düşük bir performans göstermiştir. RBF modeli, en yüksek doğruluklu derin öğrenme modeli olan RNN'e göre doğruluk oranında %12.11, keskinlik oranında ise %11.93'lük bir artış sağlamış, bu da dengesizlik arızalarının teşhisinde üstün bir araç olduğunu kanıtlamıştır. Özellikle DA\_2 sınıfında %100 doğruluk oranına ulaşarak, belirgin özellikleri sayesinde diğer sınıflardan ayırmıştır. Bu bulgular, vekil modellerin sınırlı veri gereksinimi ve düşük hesaplama maliyetiyle birlikte yüksek doğruluk ve keskinlik oranları sunarak, asenkron motor arıza teşhisinde etkili bir çözüm sunduğunu göstermektedir.

## 1. INTRODUCTION

Induction motors (IMs) are electric motors widely used in many sectors such as petroleum, automotive, and similar industries. The fact that they constitute 80% of alternating current motors in industry reveals how critically important these motors are [1, 2, 3]. Thanks to their robust structure, low maintenance requirements, and high reliability, induction motors are preferred over other types of motors. Therefore, ensuring the smooth operation of induction motors is of vital importance for the continuity of industrial processes. This is because failures in these motors can lead to serious problems such as production line stoppages, environmental damage, loss of life, and operational disruptions [4, 5, 6]. In order to prevent such negative outcomes, it is crucial to detect motor faults at an early stage. In this way, unplanned downtimes can be prevented and costly losses can be avoided [7-9].

Asynchronous motors are exposed to electrical and mechanical faults due to environmental conditions [10, 11]. Electrical faults involve the rotor and stator, while mechanical faults include bearing problems, eccentricity, and misalignment issues. 41% of motor faults originate from bearings, 36% from stators, 9% from rotors, and the remaining 14% from other causes [12].

Although rotor damages constitute a small portion of motor faults, they can lead to serious secondary problems. Rotor faults cause an increase in vibration, paving the way for bearing damage, air gap eccentricity, and winding problems. Therefore, early detection of rotor faults is critically important to prevent other faults in the motor [13, 14]. For this reason, various diagnostic techniques have been developed to detect faults [15-17].

Modern diagnostic methods for IM faults are generally based on mathematical modeling. However, these approaches are limited because full access to the system model is restricted [18]. Therefore, data-driven methods have gained popularity recently. These methods, which do not require analytical models, offer a significant advantage by eliminating the need to model complex industrial processes [19-20].

Motor faults are detected using variables such as vibration, temperature, current, and acoustics through signal processing methods. These methods include time, frequency, and time-frequency domain approaches [21-26]. The increasing amount of data has made artificial intelligence methods that provide automatic diagnosis more important. Techniques such as Artificial Neural Networks (ANN), Support Vector Machines (SVM), and

k-Nearest Neighbor (k-NN), along with feature-extracted data, perform fault detection with high accuracy [17, 24, 27, 28]. While asynchronous motor fault diagnosis faces challenges such as limited datasets and varying operating conditions, deep learning offers an effective solution to overcome these problems. In particular, pre-trained models perform well with limited data, reducing overfitting and balancing data inconsistencies under different conditions. Next-generation learning approaches enable the development of more general and adaptable models in this field, while also shortening training times and accelerating the process [29, 30].

Traditional fault diagnosis methods have long provided a reliable foundation for detecting and analyzing faults in asynchronous motors. However, in the era of Industry 4.0, where digitalization is accelerating, these methods are gradually being replaced by more innovative and flexible approaches. In this context, surrogate models emerge as an important part of this transformation [31, 32]. Also known as meta-models or response surfaces, surrogate models represent the behavior of complex physical systems using simplified mathematical or artificial intelligence-based methods and are highly advantageous in scenarios with limited data and restricted computational resources [33]. This method aims to mimic the behavior of physical systems or complex simulation models as accurately as possible. The structure of surrogate model types is shown in Figure 1. Surrogate models are generally divided into two main categories: analytical surrogate models and learned surrogate models [34].

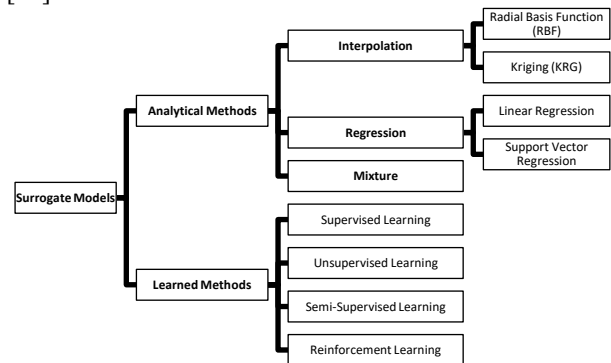


Figure 1. Surrogate Modeling Methods

Analytical models simplify complex functions using mathematical methods and typically utilize interpolation and regression techniques. While interpolation provides highly accurate predictions between data points, regression methods model the relationship between inputs and outputs to minimize the error rate. Additionally, hybrid approaches are also used. Learned models, on the other hand, operate in a data-driven manner and benefit

from large datasets. These models employ machine learning techniques such as supervised, unsupervised, and reinforcement learning, and achieve high accuracy by incorporating physical knowledge [32]. Especially for the simulation and analysis of various fault conditions in asynchronous motors, surrogate models offer a powerful tool, reducing training time and enabling the development of systems that can easily adapt to different operating conditions.

For example, Lu et al. (2019) developed a Kriging (KRG)-based surrogate model using FEM-based analysis and super-harmonic components to determine the location and depth of breathing cracks in rotating rotors. The method, optimized with particle swarm optimization (PSO), achieved over 95% accuracy with limited data and was also effective on noisy data. The study made a significant contribution to crack diagnosis by providing high accuracy at low cost [35].

Chevalier-Jabet et al. (2024) developed an ANN-based surrogate model to detect fuel rod defects in pressurized water reactors. The model, trained on 2,000 scenarios simulated with a physical model, predicted defects with a 2.6% error rate. RNN, GRU, and LSTM autoencoder models used for anomaly detection achieved 100%

accuracy, with LSTM showing superior performance especially in long data sequences. This approach contributed to real-time applications by reducing computational costs through the fast and accurate detection of fuel defects [36].

Han et al. (2013) developed a method combining a KRG surrogate model and a DE algorithm to determine bearing parameters and imbalances in rotor-bearing systems. By using a surrogate model instead of FEM, computational costs were reduced, and an error below 1% was achieved in stiffness coefficients using the differential evolution (DE) algorithm. The method provided reliable parameter identification by delivering faster and more accurate results compared to PSO and GA [37].

Yang et al. (2024) developed a surrogate model based on Radial Basis Functions (RBF), optimized with PSO, to optimize the vibration performance of tracked vehicles. The PSO-RBF model predicted vertical vibration acceleration with a 0.67% error using suspension parameters and reduced the simulation time from 670 seconds to 107 seconds. This method offers a fast and accurate solution in parameter optimization [38]. An overview of these studies is presented in Table 1.

**Table 1.** An Overview of Surrogate Model Studies

| Study                              | Method Used                     | Input  | Output – Predicted Parameters  | Output – Additional Performance Indicators                                   |
|------------------------------------|---------------------------------|--|--|--|
| Lu et al. (2019) [35]              | KRG<br>PSO, FEM                 | Sensor data<br>Finite Element Method (FEM)                           | Crack parameters (location and depth)<br>Diagnosis accuracy (95%)                          | High accuracy with limited data (95%), high performance even with noisy data |
| Chevalier-Jabet et al. (2024) [36] | RNN, GRU<br>LSTM<br>Autoencoder | Simulation and sensor data,<br>2000 scenario data                    | Activity in the coolant (2.6% error)<br>Detection of defective fuel rods                   | 2.6% error with ANN, 100% accuracy with LSTM, real-time detection            |
| Han et al. (2013) [37]             | KRG<br>DE, FEM                  | Sensor data  | Stiffness coefficients (1% error)<br>Damping coefficients                                  | %1 error   |
| Yang et al. (2024) [38]            | RBF<br>PSO                      | Vehicle suspension parameters,<br>vibration acceleration sensor data | RMS value of vibration acceleration (0.67% error)<br>Optimization of suspension parameters | 0.67% error rate   |

When the studies presented in Table 1 are examined, it is observed that KRG and RBF models are generally used for surrogate modeling. The main feature of these models is their ability to predict function values at new locations to be tested. KRG was developed based on the studies of mining engineer D.G. Krige in 1951 and holds a significant place in the field of surrogate model-based optimization. This method uses the Gaussian process to model the observed data points, enabling the prediction of complex systems and aiming to minimize the error rate [39]. The Radial Basis Function (RBF) was developed by Hardy in 1971 and later improved by Dyn and colleagues [40]. This method models the function values based on the positions of the input data and is widely used in Sequential Global Optimization (SGO) algorithms and engineering applications [41]. The RBF model is particularly successful in capturing the details of nonlinear and complex functions. KRG, on the other hand, is a powerful tool for representing both local and global trends and is

comparable to RBF in terms of accuracy [42]. In addition, Cheng and colleagues (2024) conducted a comprehensive review of data-driven surrogate model techniques developed to reduce the computational burden encountered in the design optimization process of electric motors. In the study, the performance, advantages, and limitations of statistical models (RSM, Kriging), machine learning models (SVM, RF, ANNs), and deep learning models (CNN, GAN, DNN) were evaluated. It was particularly emphasized that Kriging models can make performance predictions with high accuracy, while DL-based models stand out in handling high-dimensional design variables. This review reveals that data-based surrogate models have become not only complements to traditional analysis methods but also essential components that accelerate the design process [43].

These innovative methods have introduced a new dimension to engineering applications by increasing

accuracy while reducing computational costs. The approaches examined in the literature review will be used in the next section to develop real-time fault diagnosis methods for asynchronous motors.

This study emerged from the need to provide more accurate, faster, and cost-effective solutions against the limitations of existing methods used in the diagnosis of imbalance faults occurring in asynchronous motors. Considering the importance of real-time diagnosis in industrial fields, there is an increasing demand for approaches that can operate with limited data while offering high accuracy. In this context, the main motivation of the study is to investigate the applicability of surrogate modeling methods in diagnosing motor faults and to compare these methods with deep learning models. Furthermore, identifying models that can perform effectively even in cases where class separation is challenging will contribute to the development of decision support systems applicable in the field.

## 2. METHODOLOGY

### 2.1. Data Collection

Electrical (current signals) and mechanical (vibration velocities) performance data of the motor under different speeds and rotor fault levels were collected using the experimental setup shown in Figure 2.

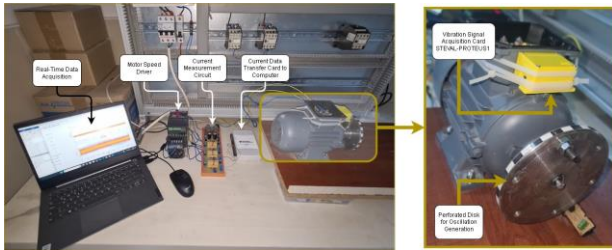


Figure 2. Experimental Setup

The dataset was obtained using a 0.37 kW asynchronous motor with the parameters specified in Table 2. The motor was examined by recording current and vibration signals for 60 seconds at different operating frequencies. Electrical fault was modeled by creating an imbalance with a disk attached to the rotor.

In the first stage, the motor was operated without any imbalance, and a dataset representing the "healthy" condition was collected. Subsequently, a screw was placed in one of the holes on the disk, and to increase vibration amplitude, a second screw was added to another hole. Using this method, a three-class dataset (Healthy, DA\_1, DA\_2) was created.

Table 2. Asynchronous Motor Parameters

| Parametre         | Değer    |
|-------------------|----------|
| Power             | 0.37 Kw  |
| Full Load Current | 1.2 A    |
| Supply Frequency  | 50 Hz    |
| Number of Poles   | 4        |
| Full Load Speed   | 1390 Rpm |
| Supply Voltage    | 380 V    |

The dataset consists of phase currents  $I_a$ ,  $I_b$ , and  $I_c$  obtained from the asynchronous motor, along with vibration signals from the X, Y, and Z axes collected via a vibration sensor. To enable the motor to operate at different speeds and to acquire various current and vibration signals, a Delta VFD007EL21A, EL-0.75kW/220V AC Motor Driver was used. The vibration signals were collected using the STEVAL-PROTEUS1 data processing card. Both current and vibration signals were recorded at a sampling frequency of 10 kHz. This dataset serves as a fundamental resource for analyzing and classifying different operating conditions of the motor, representing a significant cornerstone for analyses focused on asynchronous motor fault diagnosis.

### 2.1. Feature Extraction

The dataset includes electrical and mechanical signals for two different fault classes and one healthy class. It was created under three different load conditions, each lasting 60 seconds. The sampling frequency for vibration signals was set to 10,000 Hz, while the sampling frequency for electrical signals was 55,611 Hz. Differences in the number of samples between current and vibration signals must be synchronized to ensure accurate and reliable classification. In the literature, methods such as Windowing, Fourier Transform (FFT), Wavelet Transform, and Resampling are commonly used to align these two time series. In this study, as shown in Figure 3, the raw data (both current and vibration signals) were first subjected to data segmentation. Then, they were transformed into the frequency domain using Fourier Transform (FFT), followed by band power analysis to extract meaningful and compact features.

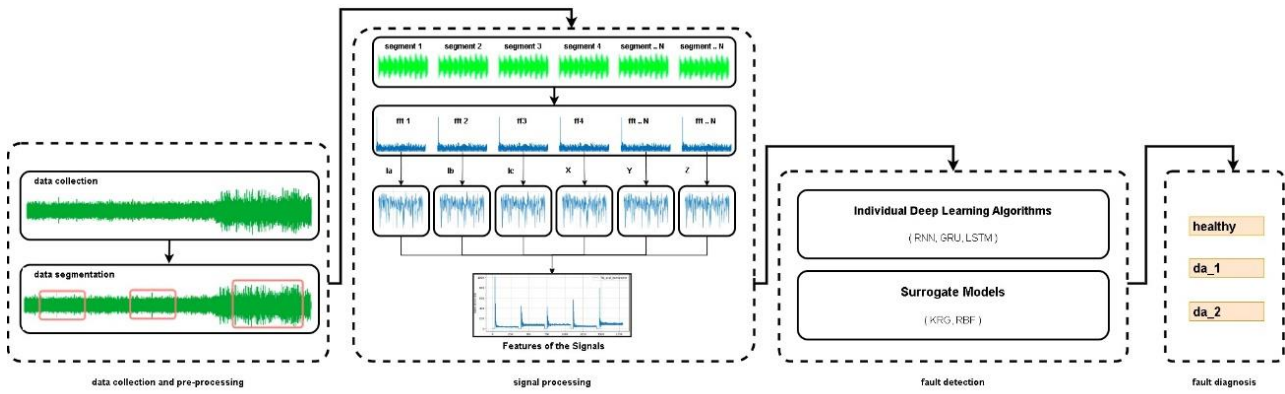


Figure 3. Signal processing, feature extraction, and classification stages

Figure 4 illustrates the signals obtained after the FFT process for current and vibration data corresponding to each output class. The visuals only display the

transformations of the Ia current and vibration signals in the X direction. Additionally, all current and vibration signals have been subjected to the same processing.

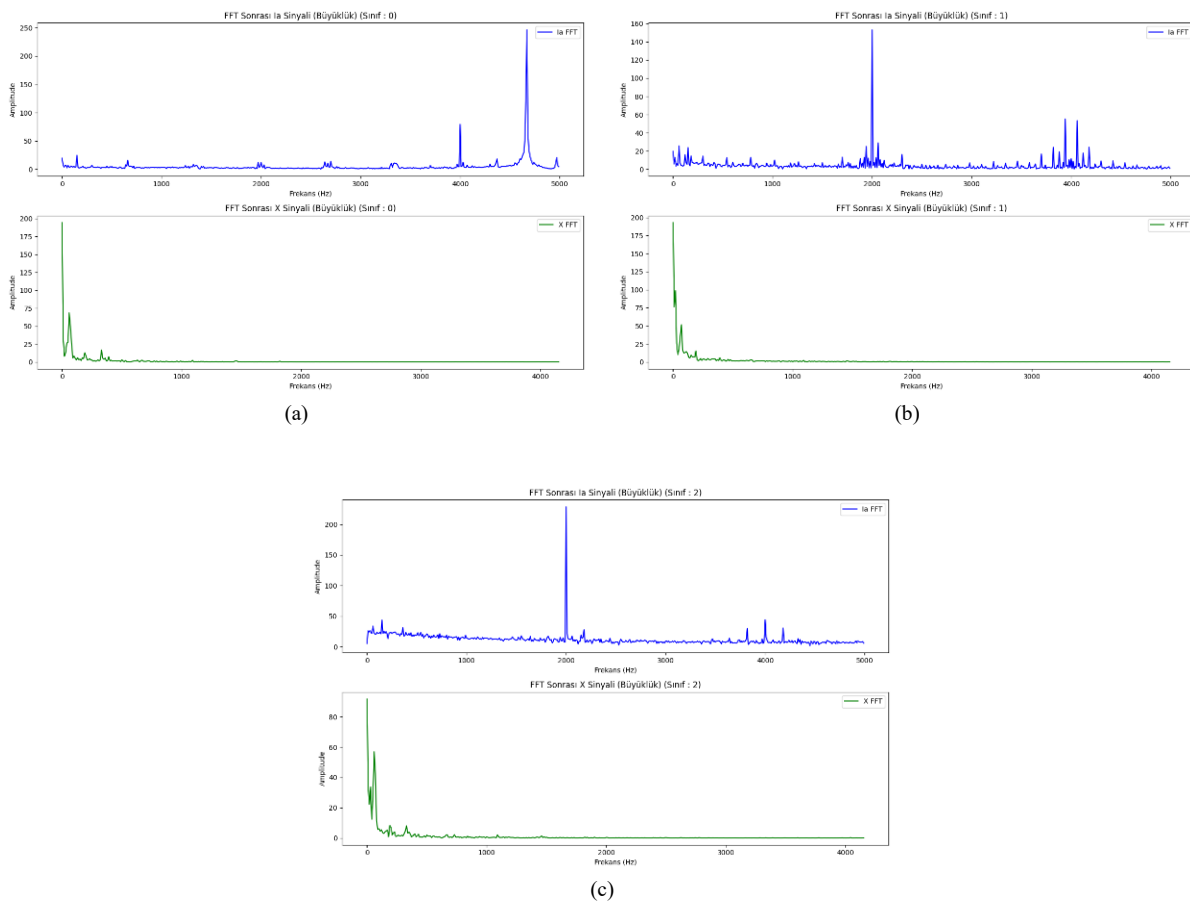
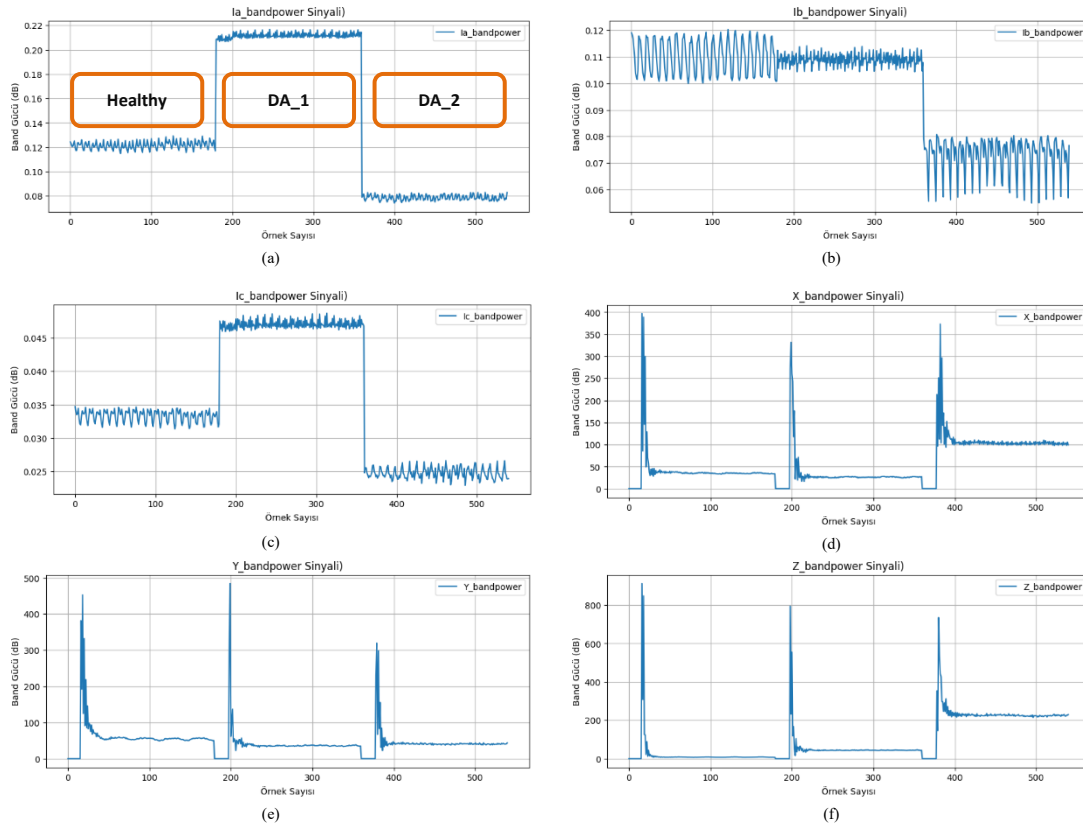


Figure 4. FFT transformation of Ia and X signals for all classes a) Healthy b) Imbalance Fault 1 (DA\_1) c) Imbalance Fault 2 (DA\_2)

The time series data were divided into predefined segment sizes, and FFT was applied to each segment. This segmentation ensured uniform processing of the data and enabled the analysis of frequency components over specific time intervals. The power spectral density (PSD) obtained through FFT was divided into specific frequency bands, summarizing the energy only within the relevant

bands. This approach facilitated the extraction of meaningful features by reducing high-dimensional and noisy data. For instance, fault-specific characteristic frequencies stood out with high energy levels in the relevant bands. Figure 5 presents the band power transformations of current and vibration data for each class label.



**Figure 5.** Combined band power transformations for all output classes a) Ia Signal b) Ib Signal c) Ic Signal d) X Signal e) Y Signal f) Z Signal

The dataset includes band power information of the current signals Ia, Ib, Ic and vibration signals X, Y, Z, as well as data related to the fault class labels. This dataset will later be used for the development of individual deep learning and surrogate model studies.

### 2.3. Classification Algorithms

#### 2.3.1. Individual deep learning models: RNN, GRU ve LSTM

RNNs are models designed to learn dependencies in sequential data and are widely used in areas such as time series analysis and signal processing. However, issues such as vanishing gradients may arise when learning long-term dependencies [44, 45]. GRU, developed to overcome this problem, controls the flow of information through gates to provide more efficient learning and stands out with its low computational cost [46, 47]. GRU is a variant of RNN developed by Chung et al. (2014) and contains gate mechanisms similar to LSTM but requires fewer parameters, making it more advantageous in terms of training time. GRU is particularly preferred in time series data due to its ability to provide high accuracy with low computational cost [48]. LSTM successfully learns long-term dependencies through its forget and output gates, although it requires a higher computational cost [49, 50]. LSTM, developed by Hochreiter and Schmidhuber (1997), is widely used in time series analysis due to its ability to learn long-term dependencies [51].

The success of LSTM- and GRU-based methods in fault diagnosis of motors has been strongly emphasized in recent studies. Lale and Yüksek (2024) compared GRU-

and LSTM-based models for diagnosing short-circuit and demagnetization faults occurring in permanent magnet synchronous motors (PMSM) and showed that the GRU model achieved 98.72% accuracy, while the LSTM model achieved 98.23% accuracy. In this study, systems modeled under different fault levels and multiple operating conditions were fed with time series-based input data, and the classification performance was found to be high. This indicates that RNN-based deep learning methods such as GRU and LSTM stand out as prominent alternatives in fault classification [52]. In this study, these three models were preferred for motor fault detection due to their ability to learn long-term dependencies.

#### 2.3.2. Surrogate learning models: RBF ve KRG

In this study, the Python-based Surrogate Modeling Toolbox (SMT) library was used to develop surrogate models, which are widely employed in the analysis of complex problems with high computational cost [53]. SMT provides a powerful and flexible framework for easily applying various surrogate modeling methods and conducting detailed analyses. Within the scope of the study, particularly the RBF and KRG methods were tested and their model performances were compared.

### 3. EXPERIMENTAL STUDIES

The experimental studies were conducted using a high-computing-capacity infrastructure to effectively handle data processing, model training, and performance evaluation processes. This infrastructure included a computer with 64 GB RAM and an NVIDIA RTX A5000 GPU with 45 GB VRAM capacity. MATLAB was

employed for data collection, while Python programming language was utilized for implementing deep learning and surrogate models. Python libraries, in particular, were used to accelerate and enhance the development of deep learning algorithms. This setup significantly improved efficiency and computational speed during model development.

For solving the classification problem, input data consisted of current signals (Ia, Ib, Ic) and vibration signals (X, Y, Z). Correspondingly, the output classes were categorized into three groups: "healthy" and imbalance faults (DA\_1, DA\_2). At the initial stage of classification, RNN, GRU, and LSTM models were individually evaluated. During model training, 90% of the

dataset was allocated for training, while the remaining 10% was used for validation and testing. To ensure reproducibility and comparability of results, the random\_state parameter was fixed at 42 across all models. The Adam algorithm, a commonly used optimization method, was chosen for training, and the learning process was limited to 50 epochs. The architecture and hyperparameters used for RNN, GRU, and LSTM models were structured consistently to ensure uniformity. Figure 6 provides detailed information about the architecture and hyperparameters of the RNN model, which were applied similarly to GRU and LSTM models. This methodology facilitated the investigation of classification performance and ensured the comparability of results.

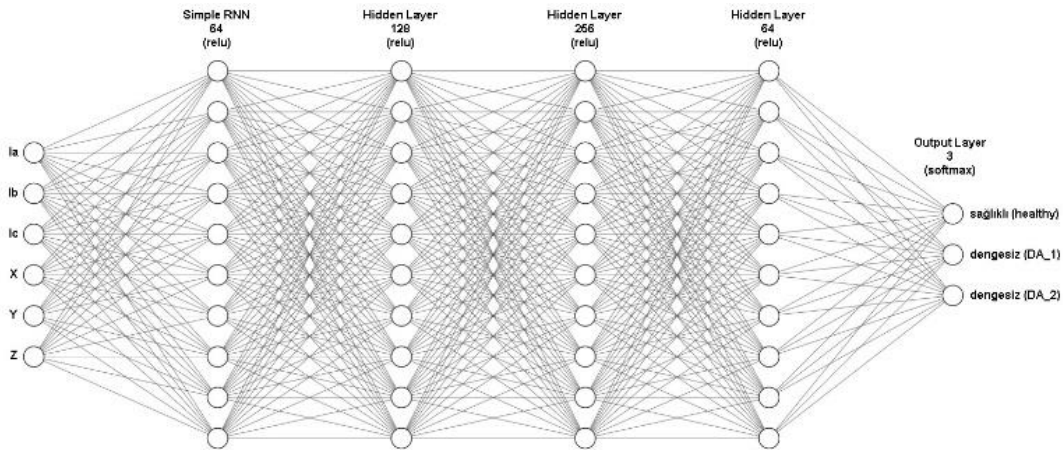


Figure 6. RNN Deep Learning Model Architecture and Hyperparameters

In the second phase of the experimental studies, RBF and KRG models were trained using the Python SMT library with appropriate parameters for each method, optimized to accurately represent the input-output relationships in the dataset. During model training, SMT's optimization tools were utilized to automatically determine each model's hyperparameters (e.g., correlation functions and kernel parameters). The trained models were evaluated on the test dataset, and their accuracy performances were analyzed in detail.

This strategy creates a separate binary classifier for each class: each model considers one class as "positive" and all other classes as "negative." A total of three different models were trained for the three classes (Healthy, DA\_1, DA\_2). When a new data sample is received, each model generates a probability output for that sample, and the class with the highest probability is predicted. This structure is illustrated in the schematic diagram below. The classification strategy related to this process is shown in Figure 7.

In this study, the "One-vs-Rest (OvR)" approach was preferred to solve the multi-class classification problem.

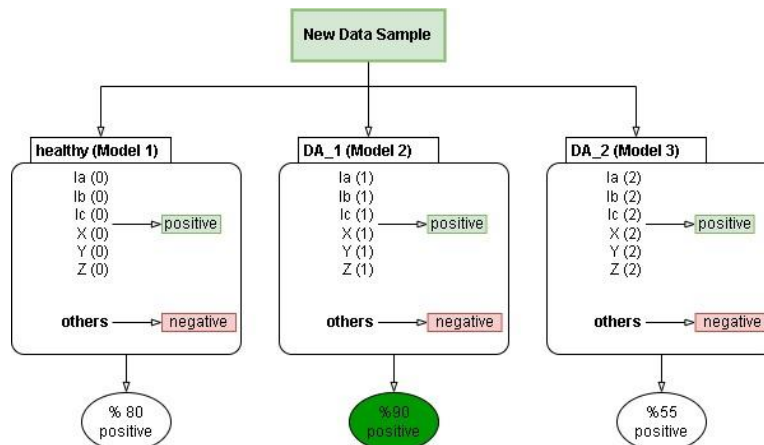


Figure 7. Modeling Classes with the One-vs-Rest Strategy

According to the strategy, each class is treated as the "positive" class, while the remaining classes are considered "negative." Since there are three classes in the study, three separate binary classifiers (models) will be created. Each model treats only one class as positive and the other two classes as negative. The implementation of the One-vs-Rest strategy is as follows:

**Model 1:** Healthy (Positive) vs. Others (DA\_1, DA\_2) : This model considers Healthy as positive based on the Ia, Ib, Ic, X, Y, Z inputs, and all remaining inputs as negative.

**Model 2:** DA\_1 (Positive) vs. Others (Healthy, DA\_2) : This model considers DA\_1 as positive based on the Ia, Ib, Ic, X, Y, Z inputs, and all remaining inputs as negative.

**Model 3:** DA\_2 (Positive) vs. Others (Healthy, DA\_1) : This model considers DA\_2 as positive based on the Ia, Ib, Ic, X, Y, Z inputs, and all remaining inputs as negative.

When a new data sample arrives, each model predicts the class membership of the sample. The class with the highest probability among the predictions determines the predicted class of the sample. For instance:

**Model 1** predicts the sample belongs to the Healthy class with an 80% probability.

**Model 2** predicts the sample belongs to the DA\_1 class with a 90% probability.

**Model 3** predicts the sample belongs to the DA\_2 class with a 55% probability.

The class with the highest probability is predicted by Model 2, indicating that the sample belongs to the DA\_1 class.

#### 4. FINDINGS

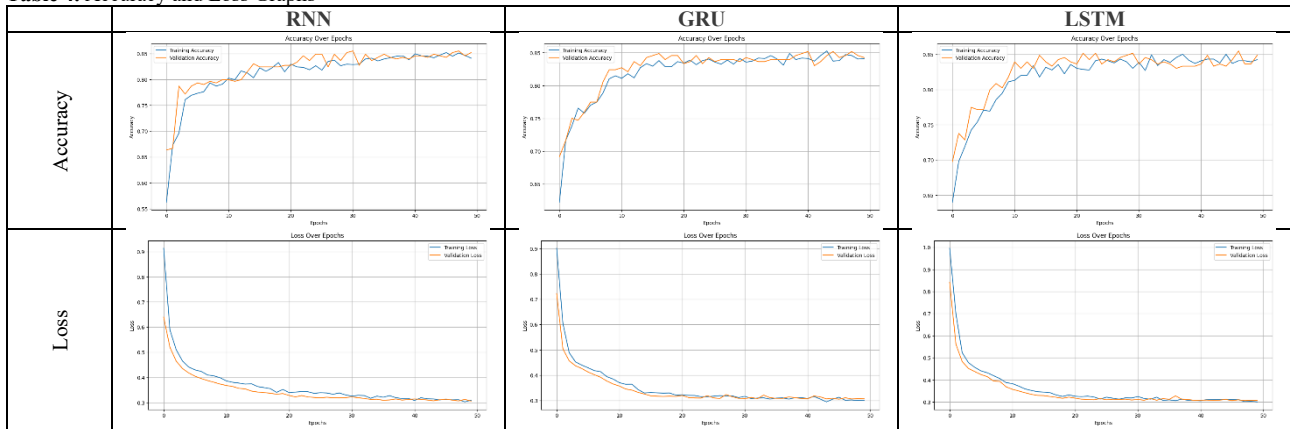
Each of the three distinct individual deep learning models aimed to approach the classification problem in the dataset from different perspectives, ensuring accurate and reliable predictions of the motor's health status. The performance results of the models are presented in Table 3.

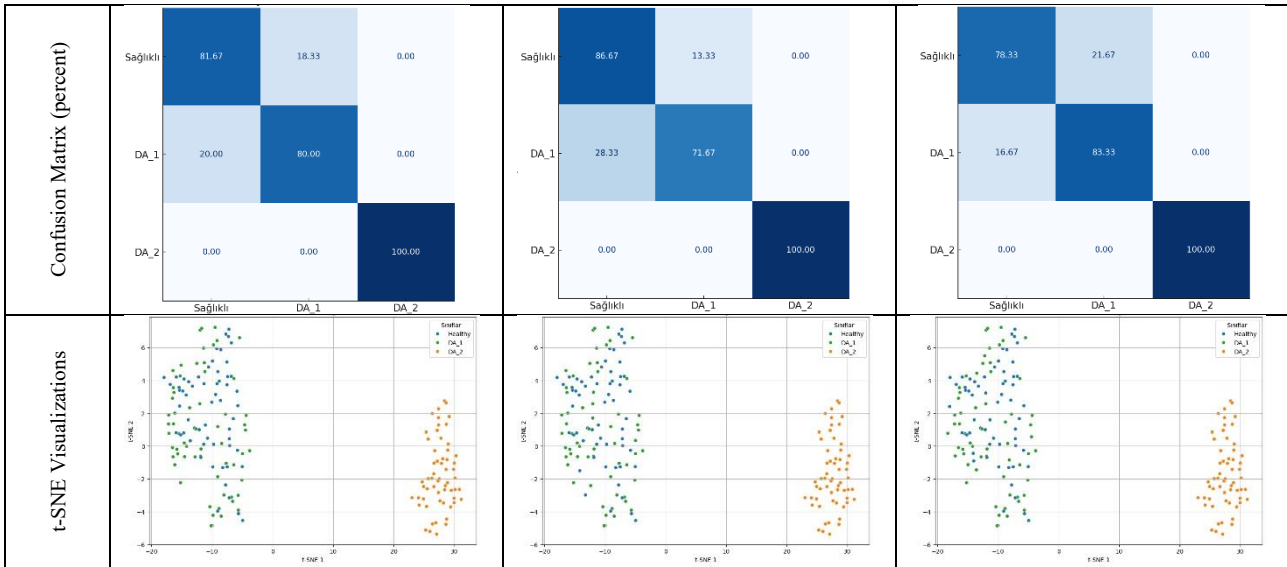
**Table 3.** Performance Results of Individual Deep Learning Models

| Model | Accuracy | Precision | Recall | F1-score |
|-------|----------|-----------|--------|----------|
| RNN   | 0.8722   | 0.8723    | 0.8722 | 0.8722   |
| GRU   | 0.8611   | 0.8656    | 0.8611 | 0.8603   |
| LSTM  | 0.8722   | 0.8727    | 0.8722 | 0.8721   |

According to the results presented in Table 3, the performance of three different deep learning models (RNN, LSTM, and GRU) in addressing the motor health classification problem was evaluated. Both the RNN and LSTM models achieved almost identical results in terms of Accuracy, Precision, Recall, and F1-Score metrics, with each demonstrating a successful performance at an accuracy rate of 87.22%. This indicates that both models effectively captured the time-series dynamics of the dataset. On the other hand, the GRU model performed slightly lower, with an accuracy rate of 86.11%, compared to RNN and LSTM. The GRU model's lower values across other metrics suggest that it was not as well-suited to the characteristics of the dataset or did not contribute as robustly to solving the classification problem as the other two models. Overall, RNN and LSTM models appear to provide more consistent and reliable results for this type of classification problem compared to the GRU model. Table 4 presents the accuracy and loss graphs, confusion matrices, and t-SNE visualizations for the models.

**Table 4.** Accuracy and Loss Graphs





According to the confusion matrices, it is observed that all models particularly struggled to distinguish between the Healthy and DA\_1 classes. The RNN model achieved an accuracy of 81.67% in the Healthy class, with 18.33% misclassification, and an accuracy of 80% in the DA\_1 class, with 20% misclassification. Similarly, the LSTM model classified the Healthy group with 78.33% accuracy and 21.67% misclassification, while achieving 83.33% accuracy and 16.67% misclassification for the DA\_1 class. The GRU model, on the other hand, demonstrated better performance for the Healthy class with 86.67% accuracy and 13.33% misclassification, but its accuracy decreased for the DA\_1 class, achieving 71.67% accuracy and 28.33% misclassification. This indicates that the Healthy and DA\_1 classes have similar characteristics, making their separation more challenging. In contrast, all models achieved error-free results for the DA\_2 class, suggesting that this class has more distinct features compared to the others.

Additionally, the t-SNE visualization results presented in Table 4 show that the DA\_2 class is clearly separated from other classes across all models. However, no clear distinction was observed between the Healthy and DA\_1 classes, as their samples are positioned in close proximity to each other. When comparing the RNN, GRU, and LSTM models, it is noted that although all models exhibited similar distributions, the GRU and LSTM models displayed more overlap between the Healthy and

DA\_1 class clusters. This further highlights the difficulty in separating the Healthy and DA\_1 classes, which impacts model performance. Notably, the clear distinction of the DA\_2 class from other classes confirms that it possesses more distinct features.

In the second phase, the results of the surrogate model approach were examined. Accordingly, Table 5 lists the performance results of the surrogate models created using the RBF and KRG methods.

**Table 5.** Surrogate Model Performance Results

| Model | Accuracy | Precision | Recall | F1-score |
|-------|----------|-----------|--------|----------|
| RBF   | 0.9778   | 0.9764    | 0.9776 | 0.9768   |
| KRG   | 0.9389   | 0.9371    | 0.9352 | 0.9360   |

According to the data in Table 5, the RBF and KRG models demonstrate impressive results, with performance exceeding 93%, establishing themselves as highly effective surrogate learning methods. The RBF model, in particular, stands out as a highly reliable and successful prediction tool due to its high metric values. Although the KRG model shows slightly lower results compared to the RBF model, it is similarly successful, and both models can be considered to provide consistent and accurate results. Table 6 presents the OvR accuracy and loss graphs, the confusion matrix, and the t-SNE visualizations for the surrogate models.

**Table 6.** Accuracy/Loss Graphs, Confusion Matrix, and t-SNE Visualizations for Surrogate Models

|                      | RBF Model   | KRG Model |        |      |      |      |      |       |      |      |      |      |        |  |          |      |      |   |          |       |      |      |      |      |       |      |      |      |      |        |  |          |      |      |
|----------------------|---|-----------|--------|------|------|------|------|-------|------|------|------|------|--------|--|----------|------|------|---|----------|-------|------|------|------|------|-------|------|------|------|------|--------|--|----------|------|------|
| Accuracy/Loss Graphs |   |           |        |      |      |      |      |       |      |      |      |      |        |  |          |      |      |   |          |       |      |      |      |      |       |      |      |      |      |        |  |          |      |      |
| Confusion Matrix     | <table border="1"> <tr> <td>Sağlıklı</td> <td>97.96</td> <td>2.04</td> <td>0.00</td> </tr> <tr> <td>DA_1</td> <td>3.12</td> <td>95.31</td> <td>1.56</td> </tr> <tr> <td>DA_2</td> <td>0.00</td> <td>0.00</td> <td>100.00</td> </tr> <tr> <td></td> <td>Sağlıklı</td> <td>DA_1</td> <td>DA_2</td> </tr> </table> | Sağlıklı  | 97.96  | 2.04 | 0.00 | DA_1 | 3.12 | 95.31 | 1.56 | DA_2 | 0.00 | 0.00 | 100.00 |  | Sağlıklı | DA_1 | DA_2 | <table border="1"> <tr> <td>Sağlıklı</td> <td>89.83</td> <td>5.93</td> <td>4.24</td> </tr> <tr> <td>DA_1</td> <td>9.26</td> <td>90.74</td> <td>0.00</td> </tr> <tr> <td>DA_2</td> <td>0.00</td> <td>0.00</td> <td>100.00</td> </tr> <tr> <td></td> <td>Sağlıklı</td> <td>DA_1</td> <td>DA_2</td> </tr> </table> | Sağlıklı | 89.83 | 5.93 | 4.24 | DA_1 | 9.26 | 90.74 | 0.00 | DA_2 | 0.00 | 0.00 | 100.00 |  | Sağlıklı | DA_1 | DA_2 |
| Sağlıklı             | 97.96   | 2.04      | 0.00   |      |      |      |      |       |      |      |      |      |        |  |          |      |      |   |          |       |      |      |      |      |       |      |      |      |      |        |  |          |      |      |
| DA_1                 | 3.12  | 95.31     | 1.56   |      |      |      |      |       |      |      |      |      |        |  |          |      |      |   |          |       |      |      |      |      |       |      |      |      |      |        |  |          |      |      |
| DA_2                 | 0.00  | 0.00      | 100.00 |      |      |      |      |       |      |      |      |      |        |  |          |      |      |   |          |       |      |      |      |      |       |      |      |      |      |        |  |          |      |      |
|                      | Sağlıklı  | DA_1      | DA_2   |      |      |      |      |       |      |      |      |      |        |  |          |      |      |   |          |       |      |      |      |      |       |      |      |      |      |        |  |          |      |      |
| Sağlıklı             | 89.83   | 5.93      | 4.24   |      |      |      |      |       |      |      |      |      |        |  |          |      |      |   |          |       |      |      |      |      |       |      |      |      |      |        |  |          |      |      |
| DA_1                 | 9.26  | 90.74     | 0.00   |      |      |      |      |       |      |      |      |      |        |  |          |      |      |   |          |       |      |      |      |      |       |      |      |      |      |        |  |          |      |      |
| DA_2                 | 0.00  | 0.00      | 100.00 |      |      |      |      |       |      |      |      |      |        |  |          |      |      |   |          |       |      |      |      |      |       |      |      |      |      |        |  |          |      |      |
|                      | Sağlıklı  | DA_1      | DA_2   |      |      |      |      |       |      |      |      |      |        |  |          |      |      |   |          |       |      |      |      |      |       |      |      |      |      |        |  |          |      |      |
| t-SNE Visualizations |   |           |        |      |      |      |      |       |      |      |      |      |        |  |          |      |      |   |          |       |      |      |      |      |       |      |      |      |      |        |  |          |      |      |

When Table 6 is examined, the accuracy and loss values for the RBF and KRG models are visualized by class. In both models, the accuracy values on a class basis are quite high, indicating the success of the classification models. The loss values are relatively low (0.01%-0.035%), which reflects that the models were well-trained during the optimization process.

Looking at the confusion matrices, the RBF model exhibits a notably high performance in the Healthy class, achieving an accuracy rate of 97.96%. Misclassifications in this class constitute 2.04%, which are shifted to the DA\_1 class. For the DA\_1 class, an accuracy rate of 95.31% was achieved, with misclassifications of 3.12% into the Healthy class and 1.56% into the DA\_2 class. In the DA\_2 class, a perfect accuracy rate of 100% was achieved, with no misclassifications. Overall, the RBF model demonstrates high performance across all classes,

although slightly more misclassifications are observed in the DA\_1 class compared to other classes.

For the KRG model, the accuracy in the Healthy class drops to 89.83%, with misclassifications of 5.93% into the DA\_1 class and 4.24% into the DA\_2 class. The DA\_1 class achieved 90.74% accuracy, with misclassifications of 9.26% into the Healthy class. Similar to the RBF model, the DA\_2 class achieved a perfect accuracy rate of 100%, with no misclassifications. The KRG model, however, exhibits lower accuracy rates in the Healthy and DA\_1 classes compared to the RBF model, while both models perform perfectly in the DA\_2 class.

Additionally, the table includes a visualization of class separability using t-SNE, showing that the DA\_2 and Healthy classes are distinctly observed as separate groups. Figure 8 presents a collective overview of the

performance results for individual deep learning and surrogate models.

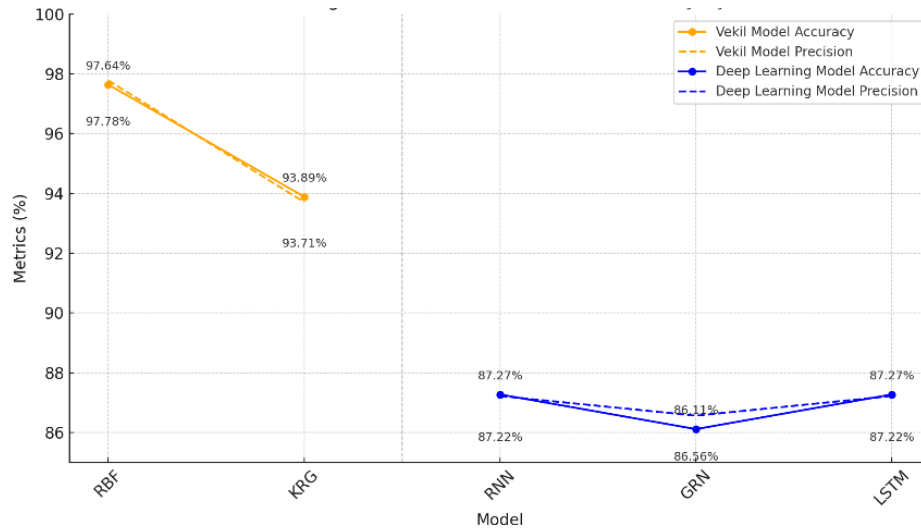


**Figure 8.** Performance results for all models

In Figure 8, a significant distinction is observed between surrogate models and individual deep learning models. When evaluated based on metrics such as Accuracy and Precision, the results clearly reveal the strengths and weaknesses of the models. Surrogate models (RBF and KRG) generally provide higher accuracy and precision values compared to other methods. In particular, the RBF model demonstrated the highest performance among all examined models, with an accuracy of 97.78% and a precision of 97.64%. The KRG model followed closely, achieving an accuracy of 93.89% and a precision of 93.71%. These findings support the capability of surrogate models to deliver high classification performance and accuracy on large datasets. Moreover, the advantages of surrogate models, such as fast computation capacity and low resource requirements, highlight their effectiveness as a dynamic alternative for use in evolving datasets.

## 5. RESULTS

This study revealed that, as a result of performance analysis of different classification models for the diagnosis of imbalance faults in asynchronous motors, surrogate learning models (RBF and KRG) achieved superior success compared to deep learning models (RNN, GRU, LSTM). The RBF model exhibited the highest performance with an accuracy of 97.78% and a precision of 97.64%, showing an increase of 12.11% in accuracy and 11.93% in precision compared to deep learning models. Similarly, the KRG model achieved notable success with an accuracy of 93.89% and a precision of 93.71%, increasing the accuracy by 6.67% and the precision by 7.44%.

In particular, the RBF model reached 100% accuracy in the DA\_2 class, enabling a clear separation of this class from the others. This proves the RBF model's success in reducing ambiguity between classes. In contrast, deep learning models made less distinct separations between the Healthy and DA\_1 classes, and the highest-

performing models, RNN and LSTM, showed lower performance with 87.22% accuracy and 87.23% precision. The GRU model, with an accuracy rate of 86.11%, produced weaker results compared to the other models.

This study provides a comprehensive evaluation not only in terms of classification performance but also regarding practical parameters such as computational cost, data requirement, and model generalizability. The ability of surrogate models to provide high accuracy even in cases of class ambiguity increases their potential for use in industrial environments. However, the sensitivity of deep learning models to data volume and their tendency for weak separation among complex classes make it necessary to support these models with hybrid structures. In future studies, it is planned to test the proposed methods on different motor types (e.g., squirrel cage motors, synchronous motors) and adapt them to the diagnosis of different fault types (e.g., bearing fault, misalignment, eccentricity). Furthermore, real-time tests will be conducted under field conditions to evaluate the operational agility and reliability levels of these models. It is also aimed to further improve classification performance and reduce training time by testing hybrid models (e.g., GRU + RBF).

## REFERENCES

- [1] Yeh, C. C., Sizov, G. Y., Sayed-Ahmed, A., Demerdash, N. A., Povinelli, R. J., Yaz, E. E., & Ionel, D. M. (2008). A reconfigurable motor for experimental emulation of stator winding interturn and broken bar faults in polyphase induction machines. *IEEE tra.*
- [2] Peroutka, Z., Glasberger, T., & Janda, M. (2009, September). Main problems and proposed solutions to induction machine drive control of multisystem locomotive. In *2009 IEEE Energy Conversion Congress and Exposition* (pp. 430-437). IEEE..

- [3] Hughes, A., & Drury, B. (2019). *Electric motors and drives: fundamentals, types and applications*. Newnes..
- [4] Rangel-Magdaleno, J., Ramirez-Cortes, J., & Peregrina-Barreto, H. (2013, May). Broken bars detection on induction motor using MCSA and mathematical morphology: An experimental study. In 2013 IEEE International Instrumentation and Measurement Technology Co.
- [5] Sen, P. C. (2021). *Principles of Electric Machines and Power Electronics, International Adaptation*. John Wiley & Sons..
- [6] Liu, Y., & Bazzi, A. M. (2017). A review and comparison of fault detection and diagnosis methods for squirrel-cage induction motors: State of the art. *ISA transactions*, 70, 400-409..
- [7] Chen, C., & Mo, C. (2004). A method for intelligent fault diagnosis of rotating machinery. *Digital Signal Processing*, 14(3), 203-217..
- [8] Talhaoui, H., Menacer, A., Kessal, A., & Tarek, A. (2018). Experimental diagnosis of broken rotor bars fault in induction machine based on Hilbert and discrete wavelet transforms. *The International Journal of Advanced Manufacturing Technology*, 95(1), 1399.
- [9] Boldea, I. (2020). *Induction Machines Handbook: Transients, Control Principles, Design and Testing*. CRC press..
- [10] Jigyasu, R., Sharma, A., Mathew, L., & Chatterji, S. (2018, June). A review of condition monitoring and fault diagnosis methods for induction motor. In 2018 Second International Conference on Intelligent Computing and Control Systems (ICICCS) (pp. 1713-17).
- [11] Nandi, S., Bharadwaj, R., Toliyat, H. A., & Parlos, A. G. (1999, October). Study of three phase induction motors with incipient rotor cage faults under different supply conditions. In *Conference Record of the 1999 IEEE Industry Applications Conference*. Th.
- [12] Nandi, S., Toliyat, H. A., & Li, X. (2005). Condition monitoring and fault diagnosis of electrical motors—A review. *IEEE transactions on energy conversion*, 20(4), 719-729..
- [13] Aydın, Ö., & Akin, E. (2024). Kırık Rotor Çubuğu Arızalarının Belirlenmesinde Derin Öğrenme Yaklaşımları ve Motor Akım İmza Analizi. *Türk Doğa ve Fen Dergisi*, 13(3), 1-7..
- [14] Hassan, O. E., Amer, M., Abdelsalam, A. K., & Williams, B. W. (2018). Induction motor broken rotor bar fault detection techniques based on fault signature analysis—a review. *IET Electric Power Applications*, 12(7), 895-907..
- [15] Dias, C. G., & Pereira, F. H. (2018). Broken rotor bars detection in induction motors running at very low slip using a Hall effect sensor. *IEEE Sensors Journal*, 18(11), 4602-4613..
- [16] Dişli, F., Gedikpınar, M., & Sengur, A. (2023). Deep transfer learning-based broken rotor fault diagnosis for Induction Motors. *Turkish Journal of Science and Technology*, 18(1), 275-290..
- [17] Aydın, I., & Akin, E. (2024, July). Multi-sensory Fault Diagnosis of Broken Rotor Bars Using Transfer Learning. In *International Conference on Intelligent and Fuzzy Systems* (pp. 349-356). Cham: Springer Nature Switzerland..
- [18] Gao, Z., Cecati, C., & Ding, S. X. (2015). A survey of fault diagnosis and fault-tolerant techniques—Part I: Fault diagnosis with model-based and signal-based approaches. *IEEE transactions on industrial electronics*, 62(6), 3757-3767..
- [19] Tariq, M. F., Khan, A. Q., Abid, M., & Mustafa, G. (2018). Data-driven robust fault detection and isolation of three-phase induction motor. *IEEE Transactions on Industrial Electronics*, 66(6), 4707-4715..
- [20] Liu, T., Luo, H., Kaynak, O., & Yin, S. (2019). A novel control-performance-oriented data-driven fault classification approach. *IEEE Systems Journal*, 14(2), 1830-1839..
- [21] Doğan, Z. (2012). *Ayrıklaştırma yöntemleri ve yapay sinir ağı kullanarak asenkron motorlarda arıza teşhisi* (Doctoral dissertation, Marmara Üniversitesi (Turkey))..
- [22] Gundewar, S. K., & Kane, P. V. (2021). Condition monitoring and fault diagnosis of induction motor. *Journal of Vibration Engineering & Technologies*, 9, 643-674..
- [23] Guo, C., Al-Shudeifat, M. A., Yan, J., Bergman, L. A., McFarland, D. M., & Butcher, E. A. (2013). Application of empirical mode decomposition to a Jeffcott rotor with a breathing crack. *Journal of Sound and Vibration*, 332(16), 3881-3892..
- [24] Dişli, F., Gedikpınar, M., & Sengur, A. (2023). Kırık Rotor Çubuğu Sayısının Ampirik Mod Ayırışımı ve Makine Öğrenmesi Yaklaşımları İle Belirlenmesi. *Fırat Üniversitesi Mühendislik Bilimleri Dergisi*, 35(2), 783-795..
- [25] Rangel-Magdaleno, J., Peregrina-Barreto, H., Ramirez-Cortes, J., Morales-Caporal, R., & Cruz-Vega, I. (2016). Vibration analysis of partially damaged rotor bar in induction motor under different load condition using DWT. *Shock and Vibration*, 2016(1), 3530.
- [26] Henao, H., Capolino, G. A., Fernandez-Cabanas, M., Filippetti, F., Bruzzese, C., Strangas, E., ... & Hedayati-Kia, S. (2014). Trends in fault diagnosis for electrical machines: A review of diagnostic techniques. *IEEE industrial electronics magazine*, 8(2),.
- [27] Rapur, J. S., & Tiwari, R. (2017). Experimental time-domain vibration-based fault diagnosis of centrifugal pumps using support vector machine. *ASCE-ASME Journal of Risk and Uncertainty in Engineering Systems, Part B: Mechanical Engineering*, 3(4), 044501..
- [28] Yang, H., Mathew, J., & Ma, L. (2005). Fault diagnosis of rolling element bearings using basis pursuit. *Mechanical Systems and Signal Processing*, 19(2), 341-356..
- [29] Jigyasu, R., Shrivastava, V., Singh, S., & Bhadoria, V. (2022, April). Transfer learning based bearing and rotor fault diagnosis of induction motor. In 2022 2nd International Conference on Advance Computing and Innovative Technologies in Engineering (ICAC).

- [30] Li, X., Zhang, W., Ding, Q., & Li, X. (2019). Diagnosing rotating machines with weakly supervised data using deep transfer learning. *IEEE transactions on industrial informatics*, 16(3), 1688-1697..
- [31] Bhosekar, A., & Ierapetritou, M. (2018). Advances in surrogate based modeling, feasibility analysis, and optimization: A review. *Computers & Chemical Engineering*, 108, 250-267..
- [32] Jiang, P., Zhou, Q., Shao, X., Jiang, P., Zhou, Q., & Shao, X. (2020). Surrogate-model-based design and optimization (pp. 135-236). Springer Singapore..
- [33] Zhou, Q., Wang, Y., Choi, S. K., Jiang, P., Shao, X., & Hu, J. (2017). A sequential multi-fidelity metamodeling approach for data regression. *Knowledge-Based Systems*, 134, 199-212..
- [34] Mohammadi, S., Bui, V. H., Su, W., & Wang, B. (2024). Surrogate Modeling for Solving OPF: A Review. *Sustainability*, 16(22), 9851..
- [35] Lu, Z., Lv, Y., & Ouyang, H. (2019). A super-harmonic feature based updating method for crack identification in rotors using a kriging surrogate model. *Applied Sciences*, 9(12), 2428..
- [36] Chevalier-Jabet, K., Verma, L., & Kremer, F. (2024). Using a surrogate model for the detection of defective PWR fuel rods. *Annals of Nuclear Energy*, 209, 110779..
- [37] Han, F., Guo, X., & Gao, H. (2013). Bearing parameter identification of rotor-bearing system based on Kriging surrogate model and evolutionary algorithm. *Journal of Sound and Vibration*, 332(11), 2659-2671..
- [38] Yang, H., Bai, X., & Wang, C. (2024). Research on surrogate models and optimization of equipment dynamics for complex systems. *AIP Advances*, 14(3)..
- [39] Krige, D. G. (1951). A statistical approach to some basic mine valuation problems on the Witwatersrand. *Journal of the Southern African Institute of Mining and Metallurgy*, 52(6), 119-139..
- [40] Hardy, R. L. (1971). Multiquadric equations of topography and other irregular surfaces. *Journal of geophysical research*, 76(8), 1905-1915..
- [41] Dyn, N., Levin, D., & Rippa, S. (1986). Numerical procedures for surface fitting of scattered data by radial functions. *SIAM Journal on Scientific and Statistical Computing*, 7(2), 639-659..
- [42] Myers, R. H., Montgomery, D. C., & Anderson-Cook, C. M. (2016). *Response surface methodology: process and product optimization using designed experiments*. John Wiley & Sons..
- [43] CHENG, Mengyu, et al. A review of data-driven surrogate models for design optimization of electric motors. *IEEE Transactions on Transportation Electrification*, 2024..
- [44] Poudel, S. (2023, August 28). Recurrent neural network (RNN) architecture explained. Medium. URL : <https://medium.com/@poudelsushmita878/recurrent-neural-network-rnn-architecture-explained-1d69560541ef> , Last Access Date : 10.12.2024.
- [45] Akbari Asanjan, A., Yang, T., Hsu, K., Sorooshian, S., Lin, J., & Peng, Q. (2018). Short-term precipitation forecast based on the PERSIANN system and LSTM recurrent neural networks. *Journal of Geophysical Research: Atmospheres*, 123(22), 12-543..
- [46] Dey, P., Hossain, E., Hossain, M. I., Chowdhury, M. A., Alam, M. S., Hossain, M. S., & Andersson, K. (2021). Comparative analysis of recurrent neural networks in stock price prediction for different frequency domains. *Algorithms*, 14(8), 251..
- [47] Anishnama. (2023, May 4). Understanding gated recurrent unit (GRU) in deep learning. Medium. URL : <https://medium.com/@anishnama20/understanding-gated-recurrent-unit-gru-in-deep-learning-2e54923f3e2> , Last Access Date : 10.12.2024.
- [48] CHUNG, Junyoung, et al. Empirical evaluation of gated recurrent neural networks on sequence modeling. *arXiv preprint arXiv:1412.3555*, 2014..
- [49] Rojas, C. A. (2024, April 8). What is LSTM (Long Short Term Memory)? Medium. URL : <https://blog.ai-evergreen.club/what-is-lstm-long-short-term-memory-221099a981f7> , Last Access Date : 10.12.2024.
- [50] Elmaz, F., Eyckerman, R., Casteels, W., Latré, S., & Hellinckx, P. (2021). CNN-LSTM architecture for predictive indoor temperature modeling. *Building and Environment*, 206, 108327.
- [51] HOCHREITER, Sepp; SCHMIDHUBER, Jürgen. Long short-term memory. *Neural computation*, 1997, 9.8: 1735-1780..
- [52] LALE, Timur; YÜKSEK, Gökhan. Identification and Classification of Turn ShortCircuit and Demagnetization Failures in PMSM Using LSTM and GRU Methods. *Bulletin of the Polish Academy of Sciences Technical Sciences*, 2024, e15158-e15158.
- [53] SMT: Surrogate Modeling Toolbox, <https://smt.readthedocs.io/en/latest/> , Last Access Date : 26.12.2024.